# Modelling and control for vibration suppression in a large flexible structure with jet thrusters and piezoactuators

F. Casella, A. Locatelli, and N. Schiavoni

Dipartimento di Elettronica e Informazione
Politecnico di Milano
Piazza L. da Vinci, 32 – 20133 Milano – Italy
e-mail: {casella, locatell, schiavon}@elet.polimi.it

*Abstract:* Active control of vibrations is a fundamental subject in the field of large flexible space structures. This paper discusses the problem of modelling and simulation of a laboratory structure equipped with both air jet thrusters and piezoactuators, which is not a trivial issue in the latter case, and proposes four different control systems, both centralised and decentralised, using either or both kind of actuators, in order to exploit their specific features at their best. Some experimental results are also presented.

## 1 Introduction

Active control of Large Space Structures (LSS) represents a vast field of research and has encouraged many theoretical and experimental works all over the world [1]. The underlying motivation is the interest in making them as light as possible for launch economy reasons, which implies the need of active vibration suppression systems, since their intrinsic stiffness and damping can be quite low. In this context, research work has been conducted for many years at the Politecnico di Milano for the development and experimental verification of active controls for a laboratory model of a LSS, a large modular truss suspended by soft springs [2]. The aim of this paper is to present some new results, and to compare different control solutions based on the use of air jet thruster actuators (AJT) and piezoelectric actuators (PA).

The paper is structured as follows: Section 2 briefly describes the experimental device; in Section 3, the model of the structure equipped with both kinds of actuator is discussed, with particular emphasis on the modelling of the structure with embedded PA's, which has some non-trivial consequences; Section 4 describes different control systems: one based on the use of the AJT only, two based on the use of the PA only (a centralised one and a decentralised one), and finally one using both at the same time. Finally, some conclusions are drawn in Section 5.

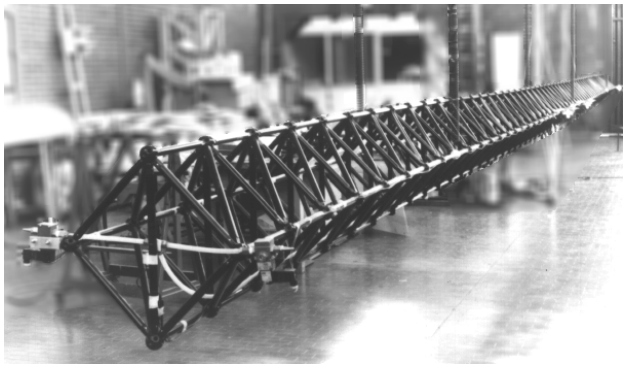

**Figure 1:** The experimental structure

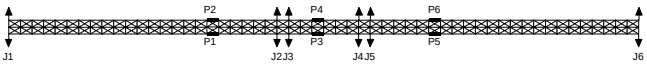


**Figure 2:** Top view of the structure with the actuators

## 2 Experimental device

The laboratory structure (Fig.1) is a linear modular truss composed of 54 bays, with a total mass of 75 kg and a total length of 19 m, built with commercial PVC elements [2]. The truss is suspended by 3 pairs of soft springs; this provides a good decoupling between the rigid and the elastic vibration modes, so that behaviour of the latter will closely resemble the dynamics in a weightless, orbital configuration. The structure has been designed so that bending modes are either in the horizontal or in the vertical plane, which permits to apply the control in the horizontal plane only, without any loss of generality.

The structure is currently equipped with twelve on-off air jet thrusters (AJT); each one of them can provide a thrust of 2.1 N. They are mounted in pairs on the structure, as shown in Fig. 2, so that, by commanding either one on the same section, a force in the horizontal plane, orthogonal to the truss main axis, can be generated in either direction. Furthermore, six piezoactuators (PA) are mounted in pairs on the structure (bays number 18, 27, and 37). Each actuator, composed of an active element and a passive connection element (Fig. 3), is mounted in the place of an ordinary structural element, providing an axial force. The actuator locations have been chosen in order to maximise the influence on the different bending modes; this subject is outside the scope of the paper, and therefore their location is considered as given.

Each kind of actuator has its own advantages and deficiencies. Air jet thrusters are very efficient in suppressing large structural vibrations, since the force they generate is aligned with the vibrational displacements of the structure; on the other hand, they also influence the overall attitude of the structure and consume fuel that must be supplied from the ground at a high cost. Piezoactuators, on the contrary, consume renewable electrical energy. Moreover, they do not influence the overall

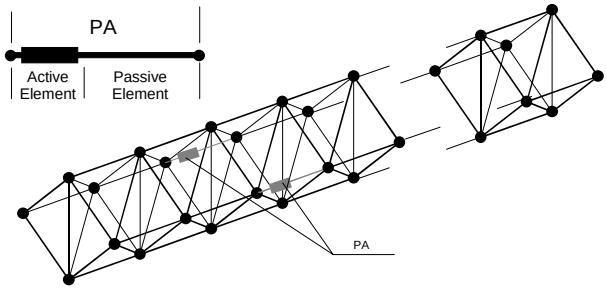


**Figure 3:** Piezoactuators mounted on the structure

attitude of the structure, since they only generate internal forces. On the other hand, they are not very efficient, as they produce a bending torque across the small transverse dimension of the structure.
Since the rigid modes of the structure are completely different from those of a free-flying one, the focus of the work will be on the suppression of vibrations relative to the bending modes. When using jet actuators, the rigid modes will be excited, and thus their motion will have to be dealt with, but only as a secondary effect. Attitude control is outside the scope of this paper.
On-board instrumentation includes six piezoresistive accelerometers, measuring the lateral acceleration of selected points of the structure, six strain gauges, measuring the axial force generated by the actuators, and six strain gauges measuring the axial extension of the active elements in the PA's. An electromechanical shaker is available for structure excitation at its natural frequencies; after the desired initial conditions have been reached, the shaker is disconnected from the structure before the control experiments begin.

# 3 Modelling

## *3.1 Modelling of the structure*

The structure is a modular truss without spinning parts, that can be modelled as if all the mass were concentrated in the $N$ nodes, connected by massless elements having the same stiffness as the connecting elements; suspension springs are modelled as equivalent springs connected to ground. Lagrange's equations of motion for such a system, assuming small displacements, can be written as follows [3]:

$$M\ddot{x} + Kx = f \tag{1}$$

where $M$ is the $N \times N$ diagonal mass matrix, $K$ is the $N \times N$ symmetrical stiffness matrix, $x$ is the $N$ vector of the node displacements in Cartesian coordinates, and $f$ is the $N$ vector of the external forces applied to the nodes in the corresponding directions. Since the structure is connected to the ground, even if with soft springs, K will be positive definite; in the case of a free-flying structure, K would only be positive semi-definite, with six zero eigenvalues corresponding to its six rigid-body degrees of freedom.
The structure under considerations has 220 nodes; therefore, Eq. (1) consists of a system of 660 coupled, second-order ordinary differential equations, that are impractical to use for numerical robustness reasons; moreover, they are far too complex to be used for control system design. A common practice is then to apply standard modal analysis concepts [3]: a linear change of variables is performed such that in the new basis the equations are uncoupled:

$$x = \Phi_c \, \eta_c \tag{2}$$

$$\ddot{\eta}_c = -\Omega_c^2 \, \eta_c + \Phi_c' \tag{3}$$

where $\eta_c$ is the $N$ vector of the modal displacements, $\Phi_c$ is the $N \times N$ matrix whose columns contain the node displacements associated to each mode (*modal participation* matrix, the prime symbol denoting matrix transposition), and $\Omega_c$ is the $N \times N$ diagonal matrix containing the natural frequencies. The matrices $\Phi_c$ and $\Omega_c$ are found by solving the eigenvalue problem:

$$K \, \Phi_c = M \, \Phi_c \, \Omega_c^2 \tag{4}$$

Displacements and velocities relative to the higher-frequency modes are usually negligible; model order reduction is therefore performed via modal truncation, i.e., only the first $n$ modes are considered. This is a crucial point, as will become clear later. The resulting simplified model is:

| # | Description | $\omega_n$ (Hz) | $\xi$ (%) |
|---|---|---|---|
| 1 | Rigid rotation | 0.2823 | 0.32 |
| 2 | Rigid translation | 0.2870 | 0.85 |
| 3 | 1st bending | 1.0356 | 0.77 |
| 4 | 2nd bending | 2.9185 | 0.94 |
| 5 | 3rd bending | 5.4506 | 1.10 |
| 6 | 4th bending | 8.9540 | 1.10 |
| 7 | 5th bending | 13.044 | 1.10 |
| 8 | 6th bending | 17.767 | 1.10 |

**Table 1.** Characteristics of the first 8 modes

$$x = \Phi \, \eta \tag{5}$$

$$\ddot{\eta} = -\Omega^2 \, \eta + \Phi' \, f \tag{6}$$

where $\eta$ is an $n$ subvector of $\eta_c$, $\Phi$ is a $N \times n$ submatrix of $\Phi_c$ and $\Omega$ is an $N \times n$ submatrix of $\Omega_c$. Numerical algorithms embedded in standard finite-element analysis software (such as MSC Nastran) compute the eigenvalues and eigenvectors of Eq. (4) one at a time in ascending order of frequency; this means that $\Omega$ and $\Phi$ can be obtained by halting the computation after a suitable number $n$ of modes has been calculated. This is particularly important in case $N$ is very large.
Eq. (1) does not take into account any dissipative effect; however, since friction is present in the real structure, a small damping coefficient should be added to Eq. (6):

$$\ddot{\eta} = -\Omega^2 \, \eta - 2 \, \Omega \, \Xi \, \dot{\eta} + \Phi' \, f \tag{7}$$

The values $\xi_{ii}$ in the diagonal matrix $\Xi$ are found experimentally by identification of the envelope of the decaying oscillations of each mode; they are reported in Tab. 1, along with the natural frequencies, for the first eight modes in the horizontal plan. The damping term is ignored in the following discussion for the sake of brevity, but has been taken into account in the model used for simulation.

## *3.2 Model of the jet actuators*

Experimental tests have shown that a delay of 12 ms exists between the application of the command voltage at the input of the AJT and the thrust generated, whereas no delay is present when the voltage is turned off. As a consequence, the duration of an impulse of thrust is 12 ms less than that of the control voltage, so that in particular no force results when the width impulse is less than 12 ms. Although conceptually simple the above description of the AJT behaviour requires a very small integration step length when simulating the system dynamics; therefore a simpler model, given by a fixed time delay of 12 ms has been used instead. Provided that no substantial control chattering arises, the results are comparable.

## *3.3 Model of the piezoactuators*

Each piezoactuator results from the series connection of a passive connection element and an active piezoelectric element. The former can be suitably described by Hooke's law, whereas in the latter the fundamental phenomena to be accounted for are the (linear) elastic behaviour and the piezoelectric effect, showing significant nonlinearity (hysteresis), which should be taken into account in an accurate model.
Let $x_1$, $x_2$ be the axial extensions of the active and passive elements, $x_p$ the total PA extension, $V$ the applied voltage, $F$ the axial force applied on the PA, $k_1$ and $k_2$ the stiffness coefficients of the active and passive elements, and $d$ the piezoelectric

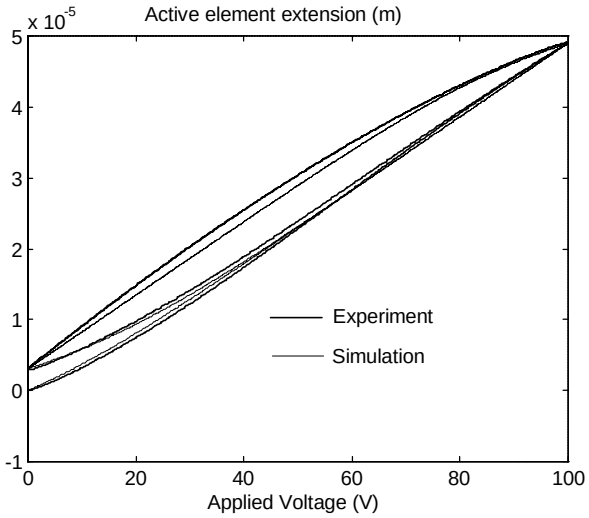


**Figure 4:** Hysteresis curve

constant. Note that $k_1 >> k_2$. The equations describing the actuators are the following:

$$x_1 = F / k_1 + V\,d + F_{hys} / k_1 \tag{8}$$

$$x_2 = F / k_2 \tag{9}$$

$$x_1 + x_2 = x_p \tag{10}$$

According to Dahl's Solid Friction model, cited in [4], the hysteresis effect can be modelled as an additional force $F_{hys}$, which is the output of the following dynamic system:

$$\dot{F}_{hys} = H\left(1 - \frac{F_{hys}}{F_c}\,\mathrm{sign}(\dot{x}_1)\right)\dot{x}_1 \tag{11}$$

The parameters $H$ and $F_c$ have been tuned experimentally, comparing real and simulated hysteresis curves (see Fig. 4). Solving equations (8)-(10), the equation describing the PA can be found:

$$F = k_p\,x_p - k_p\,V\,d - \frac{k_2}{k_1 + k_2}F_{hys} \qquad \text{with} \quad k_p = \frac{k_1\,k_2}{k_1 + k_2} \tag{12}$$

### *3.4 Model of the structure with embedded jet actuators*

Once the additional mass of the jet equipment has been included in the matrix $M$, the model of the action of a jet thruster is conceptually very simple, since it can be represented as an external force applied to the corresponding node, which in turn correspond to one or more elements of the vector $f$ in Eq. (7). If a number $n_J$ of jet actuators is present, a suitable influence matrix $M_J$ can be built such that

$$f = M_J\,u_J \tag{13}$$

where $u_J$ is the $n_J$ vector of the commands given to each on-off actuator, delayed by 12 ms.

### *3.5 Model of the structure with embedded piezoactuators*

#### 3.5.1 Model set-up

This case is much more complex than the previous one, for the following reasons:

- the actuator physically replaces one component of the structure;
- the force generated by the actuator depends not only on the control variable (i.e. the applied voltage), but also on the relative displacement between the connection nodes;
- a non-linear hysteresis effect is present.

It is desirable that the model of the structure with the embedded actuators be obtained with small modifications from the model of the original structure, i. e., taking into account the insertion of the actuators without having to modify the original $K$ and $M$ matrices and solving again eigenproblem (4). Among other things, this would facilitate tasks such as selecting the optimal actuator characteristics and positioning. In the following, the discussion will be limited to the analysis with only one actuator, for the sake of simplicity; the derivation can then be generalised to a multi-actuator configuration. The details are omitted for lack of space, but can be found in [5].

Let $x_p$ be the relative displacement between the two nodes and $F$ the axial force applied on the connecting element. In the original structure (corresponding to the original $K$ matrix), the following equation holds:

$$F = k_0\,x_p \tag{14}$$

If a PA is inserted instead of an ordinary connecting element, Eq. (12) holds instead; that can be written as:

$$F + F_a = k_0\,x_p \tag{15}$$

$$F_a = (k_0 - k_p)\,x_p + k_p\,V\,d + \frac{k_2}{k_1 + k_2}F_{hys} \tag{16}$$

that is, the action of the PA is equivalent to the original passive element plus an additional force $F_a$ acting on the PA connecting nodes. In this way, the matrix $K$ is left unchanged, and the original eigensolution ($\Phi$, $\Omega$) can still be used, while $F_a$ will enter into the vector $f$ of Eq. (7) via a suitable influence matrix.

#### 3.5.2 Non-linear analysis

The model described in the previous paragraph can be represented by the block diagram of Fig. 5. It has been verified by simulation that if the dotted path is cut, the dynamic relationship between the input $V$ and the outputs $F$, $\eta$, $a$, $x_p$ does not change significantly. The reason for this is that the piezoelectric element is much stiffer than the structure it is connected to. Therefore, it is possible to neglect the last term in Eq. (8), so that $F_{hys}$ will depend only on the voltage signal $V$, and not on the state of the structure to which the PA is connected, according to the following equation:

$$\dot{F}_{hys} = H\left(1 - \frac{F_{hys}}{F_c}\,\mathrm{sign}\left(\dot{V}\,d + \frac{\dot{F}_{hys}}{k_1}\right)\right)\cdot\left(\dot{V}\,d + \frac{\dot{F}_{hys}}{k_1}\right) \tag{17}$$

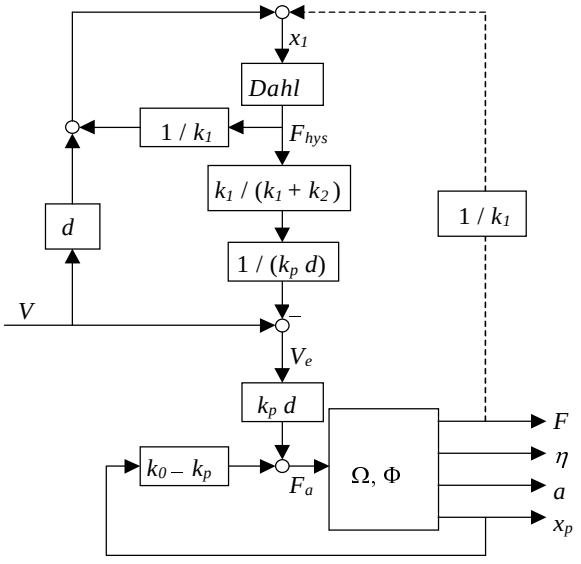


**Figure 5:** Block diagram of the structure with PA and hysteresis

Summarising, the effect of the hysteresis non-linearity is equivalent to a non-linear filter processing the applied voltage $V$. In the following analysis, the equivalent voltage $V_e$ will be considered, such that:

$$F_a = (k_0 - k_p)\, x_p + k_p\, V_e\, d\,. \tag{18}$$

3.5.3 Linear analysis via modal truncation

In the previous paragraph it has been shown that the nonlinear effects can be reduced to a suitable modification of the input signal $V$. Now it is possible to concentrate on the analyisis of the linear part of the model, whose input is $V_e$. Let $M_p$ be the influence matrix relating the actuator extensions to the displacement vector $x$, and $M_a$ the influence matrix relating the measured lateral acceleration to the displacement vector, such that:

$$f = M_p\, F_a\,; \quad x_p = M'_p\, x; \quad a = M'_a\, \ddot{x}\,. \tag{19}$$

If modal truncation is selected as the model reduction technique (as is common practice in structural analysis), the transfer function between the additional force applied by the actuator and the corresponding displacement, using the truncated modal equations (5), (6), and (19), is:

$$x_p = G_t(s)\, F_a\,, \tag{20}$$

$$G_t(s) = M'_p\, \Phi \left(sI + \Omega^2\right)^{-1} \Phi'\, M_p\,. \tag{21}$$

Solving Eqs. (15), (18), (20), and (21) for $F$, the transfer function between the applied voltage and the measured axial force is found to be:

$$F = H_t(s)\, V_e\,, \tag{22}$$

$$H_t(s) = -\frac{1 - k_0\, G_t(s)}{1 + (k_p - k_0)\, G_t(s)}\, k_p\, d\,, \tag{23}$$

while the transfer function between the applied voltage and the lateral acceleration is found to be:

$$a = P(s)\, Q(s)\, V_e\,, \tag{24}$$

$$P(s) = -\frac{k_p\, d}{1 + (k_p - k_0)\, G_t(s)}\,, \tag{25}$$

$$Q(s) = M_a\, \Phi \left[I - \Omega^2 \left(sI + \Omega^2\right)^{-1}\right]^{-1} \Phi'\, M_p\,. \tag{26}$$

It is worth noting from Eq. (23) that, in case $k_p \neq k_0$, the poles of $H_t(s)$ are different from those of $G_t(s)$: this means that the natural frequencies of the structure change with the insertion of the actuators. However, since the structural stiffness of only a few bays out of the 54 composing the structure is increased, marginal changes in the pole values might be expected. Unfortunately, the model thus obtained (comprising the first 28 modes) turns out to be completely wrong when compared to experimental data: in particular the static gain of $H_t(s)$ is wrong by a factor of eight (see [5] for details).

The failure of the model based on the truncated modal equations (5), (6), when used to deal with embedded actuators, can be traced up to the so-called Gibbs' effect [6]: when a function is approximated by an orthogonal expansion, the rate of convergence is low where the function has discontinuities: therefore, truncation can lead to large errors; a well-known occurrence of this fact is the Fourier series expansion of a triangle wave. In this case, the function to be approximated is the structural deformation vector and the orthogonal functions are the modal vectors composing matrix $\Phi$. Since the force applied by the PA leads to a sharp deformation of the truss, the corresponding node displacement will be smoothed out over several adjacent bays if a truncated model is used; this means that the computed relative displacement of the two connecting nodes will appear much smaller than real, leading to largely wrong results. On the other hand, the truncated model performs very well in the case of the force applied by the AJT's, which lead to much smoother structural deformations.

3.5.4 Linear analysis revisited

Apparently, something is wrong with modal truncation when using PA's. As a matter of fact, a vast literature exists on the subject of model reduction for flexible structures. However, the majority of them (see, e.g., [7], [8], [9]) is based on concepts such as principal component analysis and controllability and observability gramians, starting from equations which are already in modal form and already have a relatively low order for reasons of computational complexity. Therefore, the problem would not be solved, since truncation would anyway be involved. An alternative approach involves the use of the so-called Krylov vectors [10], in place of the ordinary modal vectors, in order to approximate the structure model equations. Krylov vectors lead to an approximation of $G(s)$ which preserves the first coefficients of the Laurent series expansion around $s = 0$. Correctness of the approximated transfer function at low frequency (and in particular the static gain) is guaranteed; on the other hand, the nice physical interpretation of the natural frequencies and modal shapes of modal analysis is lost; moreover, no standard commercial software tool to perform such analysis is known to the authors.

The approach taken in this work, which is rather uncommon in the field of structural analysis, is based on model residualisation, instead of model truncation. Consider the transfer function $G(s)$ between the applied force and the corresponding displacement:

$$G(s) = \sum_{i=1}^{n} \frac{a_i}{1 + s^2 / \omega_i^2} + \sum_{i=n+1}^{N} \frac{a_i}{1 + s^2 / \omega_i^2} \tag{27}$$

In the case of the AJT, the coefficients $a_i$ rapidly tend to zero with increasing $i$; conversely, this does not happen in the case of the PA. This means that the high-frequency modes give non-negligible contributions to the transfer function even at low or zero frequency, undermining the basic assumption that is taken when using the truncated model. The idea is then to approximate the contribution given by the terms of the second summation with their static gains, i.e. their steady-state behaviour, obtaining a static corrective term. The approach is sound, since the real transfer functions of the structure will show some damping and thus will be stable. Now,

$$\sum_{i=n+1}^{N} \frac{a_i}{1 + s^2 / \omega_i^2} \cong \sum_{i=n+1}^{N} a_i = G(0) - G_t(0) \tag{28}$$

so that the corrective term is

$$\tilde{G} = G(0) - G_t(0) = M_p'\, K^{-1}\, M_p - M_p'\, \Phi\, \Omega^{-2}\, \Phi'\, M_p\,. \tag{29}$$

The corrected transfer function between force and displacement is then:

$$G_c(s) = G_t(s) + \tilde{G} \tag{30}$$

In the case of a free-flying structure, both $K$ and $\Omega$ will be singular, due to the six rigid-body degrees of freedom of the structure, making Eq. (29) ill-posed. However, the problem of finding the static deformation is still well-posed, since the additional forces generated by the PA's form a balanced system, having no influence on the rigid-body degrees of freedom. It can be shown that, in this case:

$$\tilde{G} = M_{pr}' K_r^{-1} M_{pr} - M_{pr}' \Phi_r \Omega_r^{-2} \Phi_r' M_{pr} \quad (31)$$

where $M_{pr}$ and $K_r$ are obtained by removing from $M_p$ and $K$ the rows and columns corresponding to the three coordinates of two arbitrary nodes, while $\Phi_r$ and $\Omega_r$ are obtained by removing from $\Phi$ and $\Omega$ the rows and columns corresponding to the six rigid modes.

The results obtained by replacing $G_c(s)$ by $G_t(s)$ in the model (20)-(26) are highly consistent with the experimental results [5].

### *3.6 Global model of the structure with embedded actuators*

In order to obtain a model of the structure comprising all the installed actuators, a state-space model has been formulated, based on the truncated model and on the static correction term described above, generalised to the MIMO case. The linear part has been solved analytically in closed form, in order to obtain the corresponding (*A*,*B*,*C*,*D*) matrices. This model can be used for both control system design and validation by simulation. In the former case, a reduced order model (comprising the first 8 modes) can be employed wherever a low-order model is needed, while for the latter a much more accurate SIMULINK model taking into account 28 modes, hysteresis phenomena and AJT delay has been implemented.

## 4 Control design

### *4.1 Introduction*

The measurements available for vibration control are: the transverse acceleration corresponding to the AJT locations, the axial forces on the PA's, and the strain of the active elements of the PA's. In case information on the dynamic state of the structure is needed (e.g., the value of the modal coordinates up to a certain order), a suitable state estimator is employed. The estimator, originally designed in [11], employs the acceleration signals, and is based on two basic building blocks. The first is a low-pass filter, which cuts off the signal components relative to higher order unmodelled modes, in order to avoid spillover effects; the second is Kalman predictor, which estimates the modal variables corresponding to the first 8 modes on the horizontal plane (2 rigid and 6 bending); the prediction horizon compensates for the phase delay introduced by the low-pass filters. This state estimator has already been tested successfully [11], and thus has been kept unchanged for convenience.

### *4.2 Control with Jet Thrusters*

The AJT control law is shortly described here, for the sake of completeness; the interested reader is referred to [11] for details. Since the AJT are inherently ON-OFF actuator, the basic idea is to fire each of them in opposition to its velocity (a sort of "virtual friction"). This very simple controller suffers from the following drawback: in the final phase of the control transient, the actuators try to keep the structure bent out of the equilibrium position, causing high-frequency control switchings, unnecessary waste of jet fuel and actuator wear, and increased perturbation on the rigid motion of the structure.

This problem can be overcome if the truss is thought of as a collection of interconnected subsystems, each one composed by an actuator and the nearby segment of the truss. Each subsystem is subject to two kinds of forces: the local actuator thrust (having on-off nature), and the elastic force exerted by the remaining part of the structure, which is a function of its deformation state. If the accelerations caused by these two forces could be computed, then the control law of Fig. 6 could be implemented for each actuator, thus avoiding the control chattering. Since the focus is on vibration suppression of the bending modes, which are the only ones to be excited, only the corresponding velocity components should be considered; however, since the action of the AJT's could lead to (small) perturbations of the rigid modes, these too are included in the set of controlled modes, in order to stop any kind of motion completely at the end of the control transient.

Consider the dynamic model of the truss:

$$\ddot{\eta} = -\Omega^2 \eta - 2 \Omega \Xi \dot{\eta} + \Phi' M_J u \,, \quad (32)$$

$$x_c = M_a \Phi \eta, \qquad v_c = M_a \Phi \dot{\eta} \,, \quad (33)$$

where $x_c$ is the vector of the transverse displacements of the control sections (relative to the first four bending modes only), $v_c$ is the corresponding velocity vector, and $M_a$ the influence matrix transforming the vector of the node displacements into the vector of the lateral displacement of the sections where the AJT's are located. In this context, the damping term can be ignored, since the low intrinsic damping of the structure makes it negligible if compared with the control-dependent term. The dynamics of the control sections is therefore:

$$\ddot{x}_c = -M_a \Phi \Omega^2 \eta + M_a \Phi \Phi' M_J u \,; \quad (34)$$

in other words, the instantaneous lateral acceleration of each control section is the sum of two terms: the first is a function of the deformation state, the other is a function of the control variables. Provided that the actuators are sufficiently spaced from each other, the matrix $M_a \Phi \Phi' M_J$ is almost diagonal; this means that the instantaneous acceleration of a control section depends mainly on its corresponding control variable, not on the other ones. Therefore, for each actuator, the following approximate equation holds:

$$\ddot{x}_c^i \cong -k^i \eta + a^i u^i \,, \quad (35)$$

where $k_i$ is the $i$-th row of the matrix $M_a \Phi \Omega^2$ and $a_i$ is the $i$-th diagonal element of the matrix $M_a \Phi \Phi' M_J$. At this point, the control law defined in Fig. 7 can be used for each actuator, by setting $a_{el} = -k_i \eta$ and $a_c = a_i$. The algorithm actually used is slightly more complex, to deal with some actuators which are not sufficiently spaced form each other, but the underlying ideas are exactly the same. Moreover, it can be shown that the above controller is stabilising [11].

It has been verified that the experimental results agree with the simulation results, thus confirming the model correctness in a closed-loop context.

As a final remark, note that, although the idea on which this control law is based is decentralised, at least in principle, the actual controller is a centralised one, since a Kalman filter for state observation is required, and the information on the deformation of the whole structure is used to calculate every single control variable.

Figure 7 shows the result of an experiment in which all the first four modes have been excited and then controlled by the AJT control law.

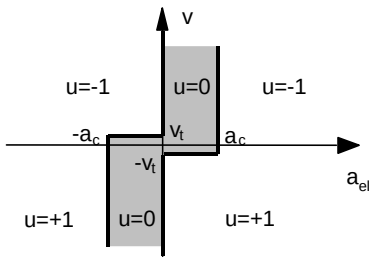


**Figure 6:** AJT Control law

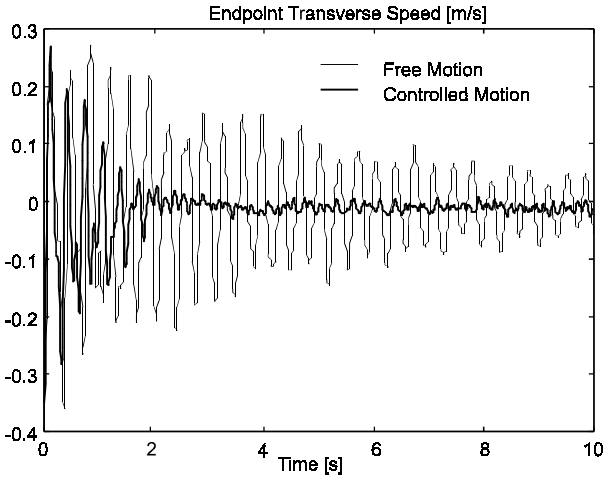


**Figure 7:** Experimental result: AJT-only controller

4.2.1 Control with Piezoactuators

When dealing with the PA's , different control strategies can be implemented, both centralised and decentralised. Some preliminary results have already been presesented in [12].

First of all, it is possible to get rid of the non-linearity by using local control loops on each PA. Following the non-linear analysis carried out in section 3.5.2, Eq. (8) can be approximated as:

$$x_1 \cong V\,d + F_{hys} / k_1 \ . \tag{36}$$

Since the frequency response between voltage and displacement is constant up to frequencies of some kHz (where the structural resonance of the PA and the amplifier poles come into action), a simple integral controller can be employed:

$$V = K_I \int_0^t (V^\circ\, d - x_1)\, dt \tag{37}$$

where $V$ is the actual voltage applied to the PA, $V^\circ$ is a "linear voltage setpoint" and $x_1$ is the actuator extension as measured by the built-in strain gauge. Within the controller bandwidth (which can be safely set around 1000 rad/s, in order to avoid interaction with the outer vibration suppression loops) the error will be approximately zero: the disturbance represented by $F_{hys}$ will be then rejected and the actuator will behave as an ideal, linear one, whose input is the setpoint $V^\circ$. This simple controller can be directly implemented by analogue devices on the same circuit of the voltage amplifier.

One may wonder how good the approximation of Eq. (36) is in terms of frequency response, since the effect of the whole truss oscillatory dynamics on the active element of the PA has been completely ignored; computations carried out on the full simulator sketched in Fig. 5 (including the dotted path) have shown that the exact frequency response differs by less than 1 dB of magnitude and less than 0.2 degrees of phase from the approximated one, in correspondence with the natural resonance peaks of the structure.

It has been verified, both by simulation and by experiments, that the introduction of these local linearising controllers noticeably improve the damping provided by the outer vibration suppression loops; moreover, the difference between the applied voltage $V$ and the setpoint $V^\circ$ is always small, i.e., no significant overvoltages are involved when closing these loops.

4.2.2 Centralised approach

The vibration suppression problem by means of the PA is intrinsically multivariable, since six actuators and six corresponding force sensors are available on the truss. The classic linear-quadratic optimal controller (LQ) is a natural candidate, since state estimation is already available. The state variables which can be controlled by the PA's correspond to the bending modes on the horizontal plane (the rigid modes can by controlled only by applying external forces). A reasonable choice is to control the first four modes. Since the hysteresis effect is rejected by the local loops described in the preceding section, and the modes above the fourth bending are made unobservable by the state estimator, a linear model based on a truncated version of Eq. (7) can be employed to synthesise the controller. This model will be cast in the state-space form:

$$\dot{x}_r = A\,x_r + B\,u\ , \quad x_r = \begin{bmatrix} \eta_r \\ \dot{\eta}_r \end{bmatrix} \tag{38}$$

where $x_r$ contains the modal variables (displacements and velocities) relative to the controlled modes and vector $u$ contains the setpoint voltages $V^\circ$ applied to the PA's. The control law

$$u = H\,x_r \tag{39}$$

is obtained by minimising the following figure of merit:

$$J = \int_0^{+\infty} (\alpha\, \eta_r'\, \Omega^2\, \eta_r + \beta\, \dot{\eta}_r'\, \dot{\eta}_r + \gamma\, u'\, B'\, B\, u)\, dt \tag{40}$$

where it can be easily shown that the term being integrated is the weighted sum of the total mechanical energy of the truss (kinetic and potential) and of the control action. The values of the modal variables $x_r$ are computed by the state estimator mentioned in Section 4.1.

The damping of the controlled structure increases with $\alpha$ and $\beta$ and decreases with $\gamma$; a compromise must be sought between a satisfactory damping and reasonable control efforts. It has been verified that the controller performance is satisfactory even in presence of (moderate) actuator saturation, despite the fact that all the theoretical properties of the LQ controller do not hold when some of the actuators saturate.

A very useful feature of this kind of controller is that, if $\alpha$ and $\beta$ are substituted with diagonal matrices, it is possible to vary the damping of the single modes independently. This can be useful in particular when using the PA's together with the AJT's, since

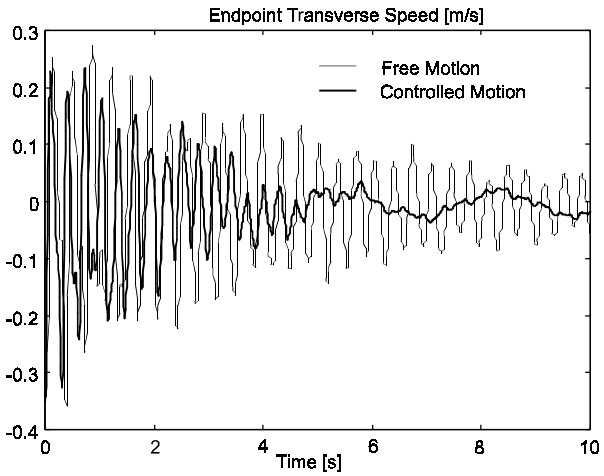


**Figure 8:** Experimental result: PA-only controller

their action is more effective on the higher frequency modes, as will be explained in section 4.4.
Figure 8 shows the result of an experiment in which all the first four modes have been excited and then controlled by the PA centralised control law. Note that the shaker used in the experiment actually excites also the rigid mode motion, and this is not controlled by the PA's; this explains the behaviour at the end of the transient.

#### 4.2.3 Decentralised approach

The controller illustrated in the preceding section finds its main strength in being centralised and strongly model-based; this permits to compute the single control variables in an optimal, co-ordinated fashion. The main drawbacks are given by the complexity of the control system (in particular of the state estimator), by the sensitivity to the model correctness and by the unpredictable behaviour in case of sensor or actuator failure. For this reasons, a simple control system has been designed as an alternative to the previous one, having a fully decentralised and co-located structure (i.e., each control voltage is a function of a measure taken on the same actuator).
The idea is to use a local force feedback on each PA; since the gain between the force on the PA and the vibrational displacement is finite, if the force is controlled to zero, so will the vibrational displacements.
The transfer function between the applied voltage and the measured force:

$$H_{tc}(s) = -\frac{1 - k_0\, G_c(\mathrm{s})}{1 + (k_p - k_0)\, G_c(\mathrm{s})}\, k_p\, d \qquad (41)$$

is not strictly proper; therefore, it is necessary to employ a low-pass controller, to obtain a loop frequency response with decreasing magnitude in order to avoid that high frequency, unmodelled dynamics destabilise the system. Supposing a single control loop is closed, it is possible to study the closed loop behaviour by means of the root locus. Poles and zeros of the transfer function (41), when the damping coefficients are included in $G_c(s)$, are located on the complex plane in pairs near the imaginary axis. Moreover, it is possible to prove that, whatever the structural parameters, the zero-pole pairs are always placed with the zero nearer the origin. The simpler transfer function leading to a root locus with the arcs connecting the zero-pole pairs orientated towards the left is a simple low-pass, first order filter. The corresponding root locus is sketched in Fig. 9 (not to scale). The cut-off frequency has been selected in order to get the maximum deviation of the root locus towards the left (the optimal choice has been 5 rad/s), while the gain has been tuned empirically, in order to avoid excessive actuator effort.
Closing many such loops at the same time (one for each actuator) could lead to unsatisfactory results, due to loop interaction. Supposing to use identically tuned controllers (with varying gain), the root locus has been computed numerically, and it has been found that its shape is not significantly different from the one obtained with a single loop, which means that loop interaction is not an issue.
Despite its simplicity, the decentralised control system leads to a performance which is comparable to that obtained with the LQ

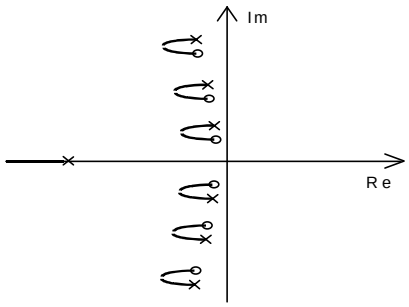


**Figure 9:** Schematic root locus

controller, and is more robust with respect to model uncertainty and sensor and actuator. On the other hand, to obtain the same increase in modal damping, about 30% more actuator energy is required, and, moreover, it is not possible to set the damping of each mode independently.
Note however that in both cases (LQ and decentralised controller) the controller had to be tuned in order to obtain relatively low gains to avoid actuator saturation, since the maximum additional force which can be exerted by the PA's is quite limited.
Table 2 summarises the performance of the two control systems, in terms of modal damping coefficients (in percent), with two different parameter tunings and with or without the local linearising loops on the PA's. These experiments have been carried out by exciting a single mode each time, and by identifying the damping coefficient as a function of the decaying rate of the structure oscillations. The experimental results are comparable to those obtained by simulation, thus validating the model soundness. Moreover, they confirm that the local linearising loops can significantly improve the overall system perfomance.

### *4.3 Combined Control*

Air jet thrusters and piezoelectric actuators possess markedly distinct features; therefore, it seems a good choice to use them in a combined fashion, in order to exploit the best features of each type. A brief analysis of the actuator features is carried out, along with suitable performance figures. The performance of the combined control system is then compared to the AJT-only and to the PA-only solution, and a controller structure is finally proposed.

#### 4.3.1 Actuator features & control system structure

The performance of the actuators can be classified according to three different criteria:

1. *Disturbance magnitude*: with the available actuators, and with the aim of controlling the vibration of the first few bending modes, the AJT's are more effective to damp out large oscillations; on the other hand, they consume non-renewable resources (fuel). Therefore, it makes sense to use them to rapidly reduce the amplitude of the vibrations resulting from large perturbations, leaving to the PA's the task of damping out vibrations of smaller amplitude

| | Free Motion | | | LQ #1 | | | LQ #2 | | | Dec. #1 | | Dec. #2 | |
|---|---|---|---|---|---|---|---|---|---|---|---|---|---|
| | $\xi_1$ | $\xi_2$ | $\xi_3$ | $\xi_1$ | $\xi_2$ | $\xi_3$ | $\xi_1$ | $\xi_2$ | $\xi_3$ | $\xi_1$ | $\xi_2$ | $\xi_1$ | $\xi_2$ |
| Local loop ON | 0.77 | 0.94 | 1.10 | 2.32 | 1.45 | 1.29 | 3.89 | 2.40 | 2.07 | 1.85 | 1.40 | 2.83 | 1.74 |
| Local loop OFF | 0.77 | 0.94 | 1.10 | 1.80 | 1.24 | 1.29 | 2.86 | 2.00 | 1.86 | 1.50 | 1.28 | 2.36 | 1.50 |

**Table 2.** Damping coefficients with different control system configurations

2. *Effectiveness on the different modes*: in the case of the AJT, the generalised force applied on the structure is a transverse force, and the corresponding generalised displacement is a transverse displacement; in the case of the PA, the generalised force applied on the structure is actually a bending torque, and the corresponding generalised displacement is the curvature of the structure. It is clear that, the transversal displacements being equal, the curvature is greater in the modes of greater order; therefore the ratio between the control effectiveness of the PA and that of the AJT increases with the mode order.
3. *Fast & accurate response*: the AJT's are characterised by delays and do not function properly if switched on and off too fast, which favours them in the control of low-frequency bending modes.

Since the actuators possess complementary features, it seems reasonable to combine two control systems using each of them, in order to obtain the best performance. The AJT control system already requires state estimation; therefore the LQ PA control system described in Section 4.3.1 has been selected, since its performance is better and the cost of state estimation has already been paid for to implement the AJT controller. Since the AJT contol system acts best on the low-frequency modes, it has been decided to let it control the two rigid modes and the first bending mode only, by removing the higher-order mode contribution from the estimate of the actuator velocity used by the control law.
The first step is to verify that, when the two control systems are operated simultaneously, no interaction results between the two, and an overall better performance is reached than with either one operated on its own; this is the subject of section 4.4.2. Then it is possible to devise a suitable supervisor which decides which control system should be operated at a given time.

4.3.2 Performance comparison of the different controllers

In order to compare the performance of the different control systems, the following experimental conditions have been selected:

1. *Initial conditions*:
   - Condition A (low frequency): the structure is excited so that the contributions to the endpoint velocity of the first four bending modes are 0.12, 0.12, 0.03, and 0.03 m/s, respectively.
   - Condition B (high frequency): the structure is excited so that the contributions to the endpoint velocity of the first four bending modes are 0.03, 0.03, 0.12, and 0.12 m/s, respectively.
2. *Active control system*
   - FM: free motion (no control system is activate).
   - J: the AJT control system is active
   - P: the PA control system is active
   - JP: both control systems are simultaneously active

To evaluate the control system performance, three figures of merit have been selected:

$$J_1 = \int_0^T u_J' \, u_J \, dt \ . \tag{42}$$

$$J_2 = \int_0^T V_{PA}' \, V_{PA} \, dt \ . \tag{43}$$

| Initial Condition | A | A | A | B | B | B |
|---|---|---|---|---|---|---|
| Controller | $J_1$ | $J_2$ | $J_3$ | $J_1$ | $J_2$ | $J_3$ |
| FM | 0.0 | 0.0 | 1.7 | 0.00 | 0.0 | 0.62 |
| J | 4.3 | 0.0 | 0.65 | 1.85 | 0.0 | 0.60 |
| P | 0.0 | 81000 | 0.65 | 0.00 | 32600 | 0.29 |
| J+P | 3.6 | 33000 | 0.33 | 0.73 | 26000 | 0.28 |

**Table 3.** Comparison of the different controller performances

$$J_3 = \int_0^T z' \, z \, dt \ . \tag{44}$$

where $T$ is the time at which the control transient is ended, $u_J$ is the AJT control vector, $V_{PA}$ is the vector of the voltages applied to the PA's, and $z$ is the stacked vector of modal displacements and velocities of the first four bending modes. $J_1$ is a measure of the fuel consumed by the AJT's to completely damp the initial perturbation, $J_2$ is a measure of the energy spent by the PA's to completely damp the initial perturbation, and $J_3$ is a measure of the effectiveness of the control action: the lesser is $J_3$, the faster is the damping of all the bending modes.
The results of the simulated experiments (in which $z$ is available for computation without any approximation) are summarised in Table 3.

Some considerations can be drawn by comparing the results:

- *Experiments starting from initial condition A*: the J+P controller performs better than the J and the P controller both in terms of energy consumption and in terms of damping performance.
- *Experiments starting from initial condition B*: the same considerations apply
- *Experiments A vs. experiments B*: the J+P controller saves control energy on the "less efficient" actuators, i.e., there's a significant saving of electrical energy when the low-frequency modes are excited more, and a significant saving of jet fuel when the high frequency modes are excited more.

Summing up, the results show that the simultaneous activation of the J and P controllers leads to good results in terms of both performance and energy consumption; moreover, they are consistent with the considerations made in Section 4.4.1.
Figure 10 shows the result of an experiment in which all the first four bending modes have been excited.

4.3.3 Combined controller structure

Once it has been verified that the simultaneous activation of the J and P controller is advantageous, it is possible to devise a hierarchical control structure, with a supervisor deciding the activation of each controller, according to the structure shown in Fig. 11. The decision criteria may vary, depending on the application.
For example, it is possible to use the total mechanical energy of the structure

$$E_M = \eta_r' \, \Omega^2 \, \eta_r + \dot{\eta}_r' \, \dot{\eta}_r \tag{46}$$

as an indicator of the magnitude of the structure perturbation, and activate the AJT control system only above a certain energy threshold. In this way, frequent, but smaller, perturbation leads to the use of the PA control system only, thus saving on jet fuel, which is employed only in the rarer case of large perturbations.

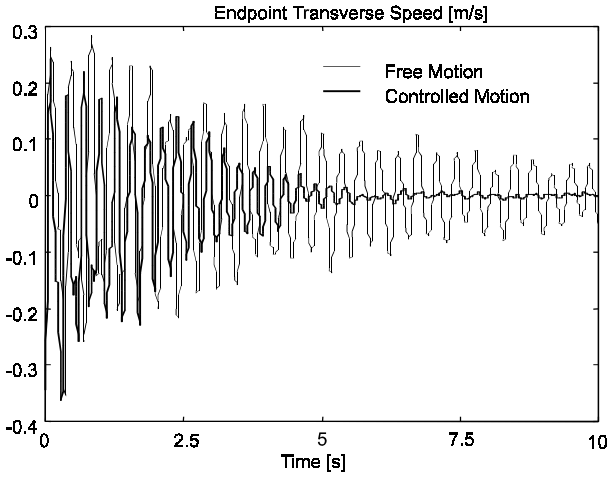


**Figure 10:** Experimental result: AJT+PA controller

The choice of the total mechanical energy as an overall indicator of the structure perturbation is the most natural, since it consistently sums up the contribution of all the bending modes, and is a rather smooth function of time, compared with all the other variables (displacements, velocities, etc.) which typically possess an oscillatory behaviour. This, together with the possible addition of a small hysteresis on the threshold, guarantees against repeated on and off switching of the AJT control system in the transition zone between large and small perturbations.

# 5 Concluding remarks

The problem of vibration suppression by means of air jet thrusters and piezoelectric actuators has been dealt with in this paper. An accurate model, including effects such as piezoelectric hysteresis and jet activation delay has been presented, both for simulation and for control system design (in its simplifed form). The correct modelling of the relationship voltage-vs.-measured force on the piezoactuators has required some non-standard analysis. Experimental results, both in open and closed loop, have confirmed the model reliability and correctness.

From the point of view of the control systems, four different configurations (AJT-only, centralised PA, decentralised PA, combined AJT+PA) have been presented and compared, in order to point out their weak and strong features. The main result is that piezoactuators are more suitable to control small vibrations of the higher order modes, while the AJT's are more efficient in suppressing large vibrations, in particular of the lower order modes. Moreover, combining the two kinds of actuators, it is possible to take advantage of the positive features of both.

The potentialities of combined control should be further investigated, although this is difficult to do without having detailed specification on the control system performance and on the mission characteristics in terms of costs and expected disturbances on the structure.

Another promising area of research, which is being investigated at present, is a study on the robustness of performance of the control system, e.g., against uncertainties in the mass distribution of the structure.

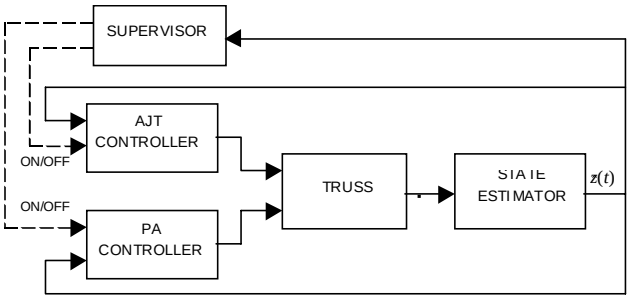


**Figure 11:** Combined controller structure

# 6 Acknowledgements

Paper partially supported by ASI (ARS-98.200), CNR, MURST (Project Idenfication and Control of Industrial Systems), Politecnico di Milano (Fondo di Ricerca d'Ateneo). The Authors thank Prof. Amalia Ercoli Finzi and Franco Bernelli-Zazzera (Dipartimento di Ingegneria Aerospaziale – Politecnico di Milano) for their support and former students Debora Londoni and Andrea Peraboni, who did some preliminary work.

# 7 References

[1] Juang, J. N. and D. W. Sparks, "Survey of Experiments ad Experimental Facilities for Control of Flexible Structures", *J. of Guidance, Control and Dynamics*, vol. 15, pp. 801-816, 1992.

[2] Ercoli-Finzi A., D. Gallieni and S. Ricci, "Design, Modal Testing and Updating of a Large Space Structure Laboratory Model (TESS)", *Proc. of the 9th VPI&SU Symposium on Structural Dynamics and Control*, Blacksburg-Virginia, pp. 409-442, 1993.

[3] Meirovitch, L., *Dynamics and Control of Structures*, J. Wiley & Sons, 1990.

[4] Hong, T. and T. N. Chang, "Control of Nonlinear Piezoelectric Stack Using Adaptive Dither", *Proc. of the American Control Conference*, Seattle, Washington USA, pp. 76-80, 1995.

[5] F. Casella, A. Locatelli, N. Schiavoni: "Modeling and Simulation of a Large Flexible Structure with Piezoelectric Actuators", *Proceedings of the 11th VPI&SU Symposium on Structural Dynamics and Control*, Blacksburg-Virginia, 1997.

[6] Baruh, H. and S. S. K. Tadikonda, "Gibbs Phenomenon in Structural Control", *J. of Guidance, Control and Dynamics*, vol. 14, pp. 51-58, 1991.

[7] Moore, B. C., "Principal Component Analysis in Linear Systems: Controllability, Observability, and Model Reduction", *IEEE Transactions on Automatic Control*, vol. AC-26, pp. 17-32, Feb. 1981.

[8] Gawronski, W, and T. Williams, "Model Reduction for Flexible Space Structures", *J. of Guidance, Control and Dynamics*, vol 14, pp. 69-76, Mar. 1991.

[9] Jonckheere, E. A., "Principal Component Analysis of Flexible Systems – Open-Loop Case", *IEEE Transactions on Automatic Control*, vol. AC-29, pp. 1095-1097, Dec. 1984.

[10] Su, T.- J. and R. R. Craig, "Model Reduction and Control of Flexible Structure Using Krylov Vectors", *J. of Guidance, Control and Dynamics*, vol. 14, pp. 260-267, Mar, 1991.

[11] F. Casella, A. Locatelli, N. Schiavoni: "Nonlinear Controllers for Vibration Suppression in a Large Flexible Structure", *Control Engineering Practice*, 4(6), pp. 791-806, 1996.

[12] F. Casella, A. Locatelli, N. Schiavoni: "Modellistica e controllo di una grande struttura flessibile con attuatori", *Atti del 41° Convegno Nazionale ANIPLA*, Torino, Nov. 1997, pp. 255-264. (In Italian)